Hidden Sector, Neutrino, and Light Matter

D. Skripachov

Abstract

The hidden sector can be used to designate phenomena that are difficult to observe, such as neutrinos, dark matter, the interior of stars and planets. Overcoming this difficulty is entrusted to simulation, in which three participants act: known facts, hypotheses, experiment. The central idea is the model of light matter (LM), according to which neutrinos are capable of forming Cooper pairs, which can then turn into bosonic nuclei of neutrinium. Experimental methods include searching for mixed pulse alternation in pulsar spectra, developing projects incl. space, based on the interactions of neutrino and LM, revising the results of collisions of accelerated protons interpreted by the creation and decay of W, Z, and Higgs bosons, as well as further study of the sources of the monochromatic signal of 3.5 keV.

1. Introduction

The hidden sector denotes a category of phenomena that make up an essential part of the world, and at the same time are difficult to observe. An example is dark matter, the total mass of which, according to astrophysical and cosmological observations, exceeds the mass of ordinary matter by 5.7 times. The energy contained in the mass of DM, paradoxically, does not manifest itself in the absorption and emission of light. Another example is the interiors of stars and planets, where difficulties in research are of the opposite nature. Meanwhile, when analyzing the spectra of galaxies observed by XMM-Newton, an unexplained excess was detected in the energy region of 3.5 keV. It was suggested that this weak monochromatic signal may indicate annihilation of DM particles interacting with each other, or the decay of hypothetical sterile neutrinos with a mass of 7 keV. However, we would be very interested to know a little more about this, in particular, how does the DM arise. This question is answered by the model of light matter (LM), which particles are the bosonic nuclei of neutrinium, consisting of neutrinos joined together. According to this model, neutrinos can experience spin-orbit interaction, the same as in Cooper electron pairs. At the same time, some of such instantaneous neutrino pairs, before decaying, turn into the LM nuclei capable of subsequent connecting with each other with the formation of more massive nuclei. Supposedly, such a synthesis of LM should be accompanied by the emission of photons with an energy of the order of several keV.

2. Hidden Sector Ontology

The hidden sector, by definition, is out of our sight. But if it exists, then it must manifest itself somehow. It means that the hidden sector can become available for observation only when we know exactly where to expect its manifestation. Following the concept of Karl Gustav Jung, we can imagine the hidden sector as an archetype of the unknown, and using the category dichotomy method, determine the location of hidden sector in the hierarchical scheme of categories (Fig. 1).

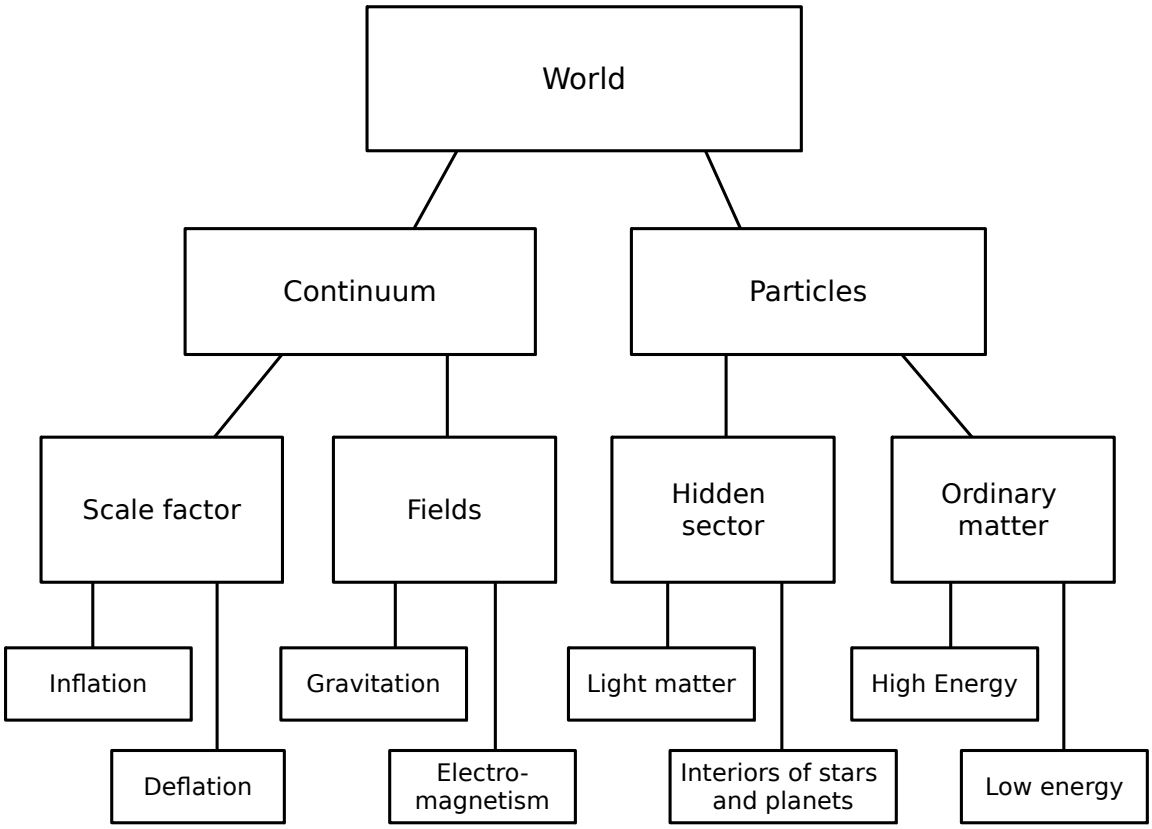

Fig. 1. The hierarchical scheme of categories.

Speaking the world, we mean everything that is accessible to our understanding. If we mean the universe, then our scheme must be supplemented with the principle of equal division of the universe into regions with matter and antimatter. In this case, we will assume that in the walls of matter the dark matter of galaxies and intergalactic matter consists of antineutrinium, and in the walls of antimatter it consists of neutrinium. In the early stage of the expansion of the universe, when the energy and density of the particles were quite high, four reactions took place between baryons and leptons, among other things:

$$p^+ + \bar{\nu} \rightarrow n^0 + e^+ \quad (1)$$

$$\bar{n}^0 + \bar{\nu} \rightarrow p^- + e^+ \quad (2)$$

$$p^- + \nu \rightarrow \bar{n}^0 + e^- \quad (3)$$

$$n^0 + \nu \rightarrow p^+ + e^- \quad (4)$$

In regions with a predominance of antineutrinium LM and antineutrino, baryons

showed a balance shift towards neutron formation, and in anti-baryons toward antiproton formation. In the regions of neutrinium LM and neutrino, on the contrary, more antineutrons and protons were formed. At the same time, annihilation occurred, more intense in charged baryons. As a result, baryons began to predominate in areas with antineutrinium LM, and, on the contrary, antibaryons in regions with neutrinium LM.

The alternation of galactic walls and filaments separated by voids can be likened to foam with cells in the form of truncated octahedra. In a package of truncated octahedrons, filament ribs are located at the intersection of three wall faces, so that two walls of matter (antimatter) form a filament. The third wall, consisting of antimatter (matter), is separated from the filament by a gap of a very rarefied, almost empty space, as in voids. The thickness of such gaps is assumed to be comparable with the thickness of the filaments.

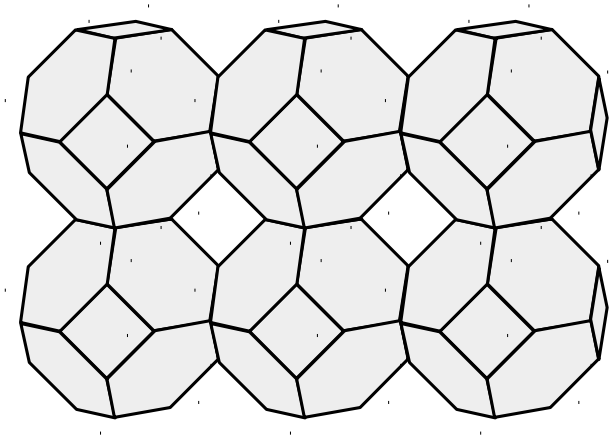

Fig. 2. Packing truncated octahedra.

Such a large-scale separation of matter and antimatter, however, cannot be absolute, and in galaxies there should be some slight residual mixing of matter with antimatter and vice versa.

3. Properties of Light Matter

According to the LM model, between neutrinos, when they approach each other by a distance of the order of 10^{-9} cm a spin–orbit interaction occurs. As a result of this, instantaneous neutrino pairs arise. The spin-orbit interaction between neutrinos only occurs when the orbital moment is opposite to the helicity of the neutrino. Accordingly, the spin of such neutrino pairs turns out to be zero.

As soon as neutrinos diverge from each other, most pairs decay. But in some cases, with a closer convergence and an optimal angle of intersection of the trajectories (presumably 15-25°), neutrino pairs may experience fusion with the transformation into the bosonic nuclei of neutrinium:

$$\nu_1 + \nu_2 \rightarrow {}^{2}Nu + \gamma \qquad (5)$$

It is assumed, that such newly formed nuclei have a spin equal to 1. The radiation energy during the fusion is estimated to be up to 0.5% of the energy of the initial neutrinos.

It is assumed that neutrinos in the LM nuclei confirm their kinship with the electrons through the relative proximity of the component masses to the rest mass of the electron. Based on this assertion, we will assume that the rest mass of dutrinium (^{2}Nu or Du) is in the range of 0.6-0.8 MeV.

Dutrinium is capable of synthesizing heavier nuclei:

$$Du + Du \rightarrow {}^{4}Nu + \gamma \tag{6}$$

$$Du + {}^{4}Nu \rightarrow {}^{6}Nu + \gamma \tag{7}$$

The spatial configuration of the neutrinium nuclei is derived from the assumed cubic form of the neutrino and the linkage principle along the edges of cubes. Moreover, it is assumed that both of the two unit cells of space related to a given link of two neutrinos do not participate in other links of any of these neutrinos with other neutrinos (Fig. 3, g).

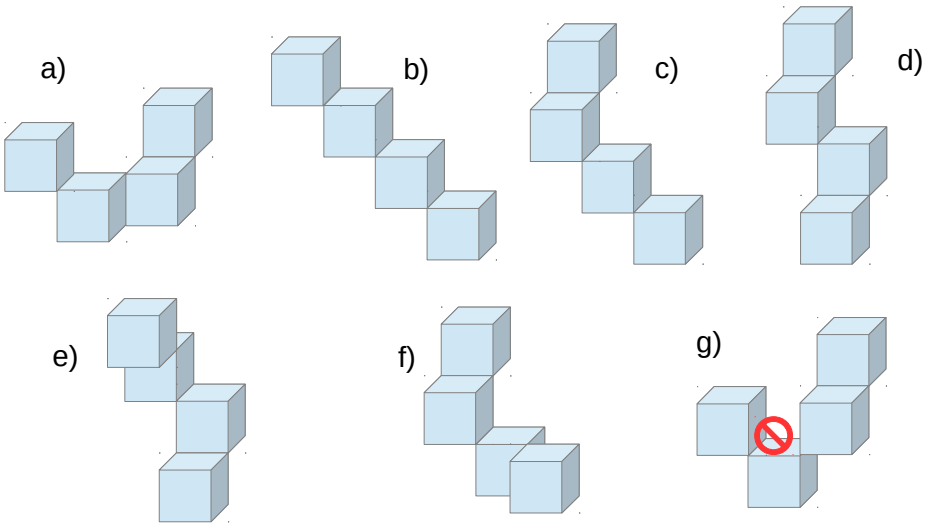

Fig. 3. Configurations of tetrinium isomers

Let us denote the neutrino link along the edges of cubes as an alpha bond. For neutrinos connected by an α bond, the concepts of valency and covalence are applicable. The neutrino valency (the number of actually present α-bonds) can be 1, 2 or 3, and the covalency (the maximum possible number of α-bonds of a neutrino in this position) is 2 or 3. In the linear isomer (Fig. 3, b) there are two internal neutrinos have a valency of 2 and a covalency of 2, that is, they are completely saturated, unable to form new α-bonds. In the partially linear and branched isomer (Fig. 1, c), one internal neutrino has covalency 2 and the other covalency 3. In the remaining four branched isomers, both internal neutrinos have covalency 3. Preferring a more symmetrical form, we assume that tetrinium has form a).

For hexatrinium, the symmetric 6-membered cycle appears to be the most preferred.

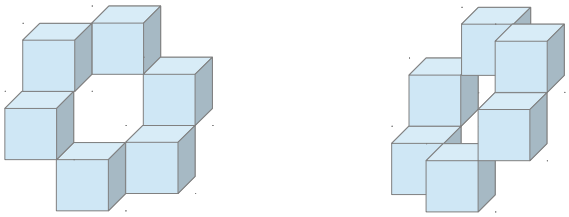

Fig. 4. Configuration of hexatrinium

The continuation of a number of elements of LM suggests that one of the neutrinos must have a valency of 3. However, with increasing valency, the strength of the bonds between neutrinos decreases, and this means that nuclei with too many pairs can be unstable. Therefore, we will assume that the synthesis of LM ends with hexatrinium.

Thus, we found that LM consists of three types of nuclei (Table 1).

Table 1: Neutrinium Elements of Light Matter.

Neutrino number	Designation	Name	Mass, MeV/s^2	Spin
2	^{2}Nu, Du	Dutrinium	~0.7	1
4	^{4}Nu, Tt	Tetrinium	~1.4	0
6	^{6}Nu, Hx	Hexatrinium	~2.1	1

It should be noted that along with the synthesis, the following reversible exchange reaction is possible:

$$Tt + Tt \Leftrightarrow Hx + Du \tag{8}$$

In a strong magnetic field, nuclei of LM with nonzero spin will tend to occupy an orientation along the magnetic field lines. In this case, magnetic resonance will occur, and the LM nuclei can emit. The spectrum of such radiation depends on the temperature of LM and, to a lesser extent, on the magnetic field strength. It is assumed that the energy of quanta of such magnetic resonance radiation will be approximately 1.9×10^8 times less than that of thermal radiation. The radiation intensity depends on the density of LM, and on the strength and uniformity of the magnetic field. It is also assumed that the direction of this radiation is concentrated in a plane perpendicular to the magnetic lines of force.

With sufficient proximity, the nuclei of LM and anti-LM can annihilate:

$$Du + \bar{Du} \rightarrow 2\gamma\ , \tag{9}$$

$$Du + \bar{T}t \rightarrow 2\bar{\nu} + 2\gamma \,, \tag{10}$$

$$Du + \bar{H}x \rightarrow \bar{D}u + 2\bar{\nu} + 2\gamma \,, \tag{11}$$

$$Hx + \bar{H}x \rightarrow Du + \bar{D}u + 2\nu + 2\bar{\nu} + 2\gamma \,, \tag{12}$$

Annihilation is accompanied by radiation of a wide spectrum, from IR to γ-rays. In a strong and uniform magnetic field, the probability of annihilation of LM nuclei with nonzero spin increases significantly. This is due to the emergence of instantaneous pairs of LM-anti-LM nuclei, which can be spaced a considerable distance, orders of magnitude larger than the dimensions of the LM nuclei themselves.

4. Light Matter in the Solar System

Under the action of gravitation of the Sun, part of the galactic LM experiences accretion on the Sun. Accretion parameters are given in Table 2.

Table 2: LM Accretion Parameters in the Solar System.

Parameter	Value
The speed of rotation of the Sun around the galactic center	~230 km/s
Acceleration of free fall on the galactic center	2.11×10^{-10} m/s^2
LM density at the galactocentric radius of the Sun	0.43 GeV/s^2/cm^3
Accretion sphere radius	5300 AU
First cosmic velocity at the accretion boundary	409 m/s
The spherical angle where the velocity of LM relative to the Sun is equal to the first cosmic velocity at the accretion boundary	π/1765
Coefficient taking into account the coincidence of the direction of motion of LM with the rotation of the Galaxy	2
The density of the part of LM captured by the gravitation of the Sun, on the radius of the accretion sphere	6.8×10^{-7} GeV/s^2/cm^3

To find the density of the accreting LM, we apply the same law of the density distribution of LM, as on the scale of the Galaxy:

$$\rho_{LM}(r) = \rho_{NS}\,(r_{NS}/r)^{2.5} \,, \tag{13}$$

where
r_{NS} is estimated radius of a conditional neutron star with the mass of the Sun,
ρ_{NS} is density of LM on the surface of the conditional neutron star.

Assuming the density of neutron matter to be 5.0×10^{17} kg/m^3, we find that the radius of a neutron star with a mass of the Sun is 9.83 km. The value of the LM density on the neutron star surface is taken to be 2.24 kg/m^3 (chosen arbitrarily to obtain a coincidence of the calculated value with the calculated density of a portion of LM at the accretion boundary).

Using formula (13), we find that the density of LM increases 2 times relative to the average density of the galactic LM between the orbits of Uranus and Neptune, and closer to the Sun it is:

- 1.4×10^{3} GeV/s^2/cm^3 at the distance of 1 AU,
- 9.4×10^{8} GeV/s^2/cm^3 on the surface of the Sun.

If we assume that the LM density inside the Sun is constant, then the mass of the galactic LM inside the Sun will be 1.2×10^{-15} $M_\odot$.

The rate of accretion of the galactic LM on the surface of the Sun is conventionally defined as 20% of the galactic LM present there, which rushes inward from the surface of the Sun at the first cosmic velocity per unit time. This rate is about 10^6 kg per second.

The effective cross section for the collision of LM nuclei with each other and with atoms of ordinary matter is taken to be 14 orders of magnitude smaller than that of atoms and molecules. The equivalent density of solar gas for LM will be the same as that of atoms and molecules in the Earth's atmosphere at an altitude of 320 km. Then the average path length of LM nuclei inside the Sun will be several kilometers. This means that the galactic LM falling on the Sun for a time of the order of several tens of seconds becomes part of the solar substance.

The observed deficit of solar neutrinos is explained by their transition into LM. A neutrino deficit of 60% means that every second about 10^8 kg of primary solar dutrinium is synthesized inside the Sun. This value is two orders of magnitude larger than the influx of galactic LM. Reaching the photosphere, the neutrinium LM, as well as the antineutrinium LM of galactic origin are scattered into the surrounding space. However, the escape velocity of the scattering LM is insufficient to overcome the gravitation of the Sun, and most LM (conditionally 80% or more) remain to circulate in the halo around the Sun.

The synthesis of Tt, Hx from slow Du near the Sun is supposedly the main factor in heating the solar corona. This synthesis should be accompanied by radiation with an energy of 1-2 keV.

While most of solar LM (conditionally 98-99%) is synthesized inside the Sun, a small part (less then 2%) is synthesized in the photosphere and corona. This part is a fast Du, synthesized in the same way, mainly from pp neutrinos. Fast Du leaves the Sun as part of the solar wind. However, some of it connects in the corona with slow Du, Tt, giving the output Tt, Hx. And this synthesis is accompanied by radiation with an energy of 3.5-3.6 keV.

It is assumed that a significant part of LM (conditionally 50% of the galactic and 0.5% of the solar) annihilates on the Sun. LM annihilation is accompanied by the emission of secondary neutrinos. Annihilation is more intense in areas of a strong magnetic field, particularly in prominences and in coronal loops. Over these regions, zones of intersection of neutrino fluxes arise. Helmet streamers above these zones may indicate enhanced synthesis of LM.

5. Hidden Sector on Earth, Jupiter

Observation of the phenomena of the hidden sector implies a commensurability of the scale of the observation region and the volume of the medium in which it is expected to occur. So, the appearance and decay of instantaneous neutrino-electron pairs occurs everywhere and can be accompanied by radio emission. This radio emission is part of the natural background of the environment. A recent study of data from seismometers on the ocean floor has led to the identification of constant fluctuations in the background noise of the Earth at a frequency of 2.9-4.5 milli-

hertz. It is difficult to find for these oscillations an explanation in internal processes inside the Earth, and the only explanation is that these oscillations reflect changes in the flux density of solar neutrinos. It is assumed that in this case, fluctuations in background noise should correlate with fluctuations in brightness of the corona.

The effects of LM are manifested in the atmosphere, in particular, during thunderstorms. Blue jets, sprites and elves are likely to result from the annihilation of LM induced by the lightning magnetic field.

The source of aurora kilometric radiation is probably LM. If we assume the near-Earth LM temperature equal to 300 K, then the spectral maximum of the LM polar radio emission will be 163 kHz.

In the circumpolar regions, the magnetic field favors the annihilation of LM. Near Jupiter, the density of LM is 50-100 times higher than that of the Earth, and also there is a higher magnetic field strength. Bright x-ray radiation in the polar regions of Jupiter is due to the annihilation of galactic and solar LM. At the Earth, ozone holes can be caused by the annihilation of LM. Moreover, near the Earth, the flux density of fast solar LM is higher. Annihilation between fast solar and slow galactic LM can be considered as an alternative source of theta aurora.

6. Radio Pulsars

Near any neutron star, soon after birth, a dense halo is formed from neutrinium LM, that has been accumulated around the predecessor star during its life cycle. For a neutron star with a mass of 1.5 $M_\odot$ and an average radius of 12 km, the LM density in the halo above the surface of the star can reach 4 kg/m^3. The average path length of LM nuclei in such a dense halo will be about 2 thousand km. At the same time, the depth of penetration of LM into the crust of the neutron star does not exceed several tens of meters. Between the crust of a rapidly rotating neutron star and also rotating but more slowly, the halo of LM, friction occurs which excites an electric current in the crust. This electric current finds a shorter path and creates a theta pinch, which stimulates the neutron star to take the shape of a three-axis ellipsoid. The magnetic poles are shifted towards the equatorial protrusions. Above the magnetic poles at an altitude of 5 to 20 km, LM generates magnetically induced radiation. At a temperature of 600000 K, the radio emission from LM has a maximum at a frequency of 327 MHz.

The gravitation of the neutron star bends the planes of radio emission, and they turn into two wide-angle conical surfaces with an aperture of 170 degrees (Fig. 5).

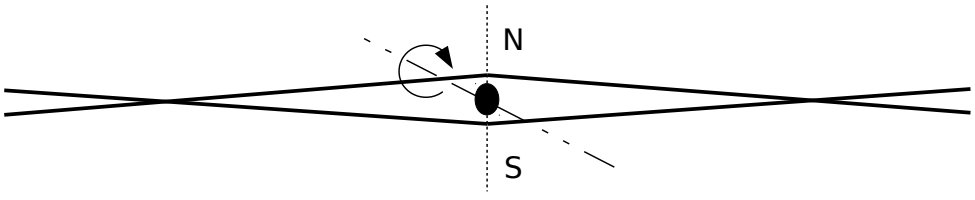

Fig. 5. Two conical surfaces of the pulsar’s radio emission

In the profile of each pulse, the earlier peak corresponds to the frontal di-

rection of radiation, and the main part of the pulse corresponds to the rear direction. The difference in power is due to the fact that the thickness of the active region in the rear direction is significantly greater than in the frontal direction.

Together with a neutron star, the LM halo also rotates. Halo rotation leads to the fact that the early peak has a blue shift, and the main pulse has a red shift. In the directions perpendicular to the axis of rotation, the magnitude of shift has a maximum with a value of about z≈2.

A slight decrease in the frequency during the main pulse is due to the instantaneous cooling of the radiation region.

Both the crust and the core of the neutron star are characterized by a polycrystalline structure, which gives the star a certain rigidity. Glitches of pulsars signal a restructuring that occurs when the difference between centrifugal forces and gravitation begins to exceed the yield strength of a neutron star.

The larger the mass of the neutron star, the greater the gravitational curvature of the magnetic field lines, and they enter the star closer to the magnetic equator. With a mass of about 2 $M_\odot$, demagnetization regions can appear at the magnetic poles. In the pulse profile, this effect corresponds to two early peaks with a consistently single main pulse (as in PSR J0348+0432). With an even larger mass (> 2.2 $M_\odot$) gravitation completely dampens the star's magnetic field.

7. Quasars and Jets

In the two-level mass model of the Milky Way, a decrease in the density of LM in the central part of the galaxy was explained by heating and scattering of the galactic LM as a result of annihilation of native antineutrinium LM with an admixture of neutrinium anti-LM. The content of this admixture may vary. The active galaxy nuclei and quasars are characterized by a higher content of anti-LM mixing. To estimate the content of anti-LM admixture in quasars, we take the quasar 3C 273 as a model and apply to it the density distribution of LM in the center of our Galaxy. As in the case of the Sun, we will take the effective cross section for the collision of LM nuclei to be 14 orders of magnitude smaller than for atoms and molecules. Exemplary LM parameters for the proposed range of annihilation localization in AGN and quasars are shown in the Table 3.

Table 3: Parameters of LM in the center of a galaxy similar to the Milky Way

Distance from the center, AU	LM density, kg/m^3	LM nuclei average speed, km/s	Average travel time
1	2.2	14130	0.27 seconds
10	7.0×10^{-3}	6170	3.2 minutes
100	2.2×10^{-5}	3080	1.4 days
1000	7.0×10^{-8}	1660	2.3 years

Burnout of anti-LM can be distributed as follows:

- 75% in the lower layers of the halo between 1 and 100 AU,
- 20% in the middle layers of the halo between 100 and 1000 AU,
- 5% or less at distances above 1000 AU.

The rate of accretion of LM to the center of a galaxy similar to the Milky Way is

defined as 10% of the mass of LM falling from a distance of 100 AU at the first cosmic velocity per unit time. This rate will be 2×10^{28} kg per second.

The radiation power of the quasar 3C 273 is approximately 4.1×10^{12} times greater than the radiation of the Sun. Accordingly, the necessary energy from the annihilation of LM is achieved when the content of anti-LM admixture is 2 ppm.

In a dense medium of LM, gamma photons should have a mean free path comparable with the mean free path of LM nuclei. This means that up to 80% of the initial gamma radiation generated in dense layers is scattered by the halo of LM and re-emitted in the longer wavelength spectrum.

Relativistic jets can make up a significant portion of quasar radiation. Jets arise during the annihilation of LM in a uniform magnetic field in the region of magnetic poles. In turn, the magnetic field arises as a result of the motion of the LM and hot gas. In the presence of a magnetic field, a direct collision of LM nuclei is no longer a necessary factor and annihilation occurs in a more rarefied medium, with a density of LM from 10^{-16} kg/m^3 . This corresponds to an area bounded by a radius of 20 parsecs. Accordingly, the initial diameter of relativistic jets generated in this area at the magnetic poles will be about 10 parsecs.

8. Experimental Methods

The description of the phenomena in the previous chapters, made from the point of view of the participation of a hypothetical LM, can be characterized as a simulation. The simulation will continue to offer promising experiments. Let's review these experiments briefly.

1) Analysis of pulsar spectra with an even-odd mixed pulse alternation search algorithm. Revealing a mixed (rather than simple) alternation of pulses will make it possible to prove that the radio emission of pulsars has the shape of wide-open (almost flat) conical surfaces, rather than narrow cones.

2) Generation and reception of radio emission from LM. It requires a long plastic pipe with large diameter. The pipe is shielded with a copper or aluminum screen. Outside, two rows of neodymium or electric magnets are installed along the pipe. At the ends of the pipe, radio antennas are installed. The range of expected radio emission is from 30 kHz to 3 MHz.

3) The interaction of solar neutrinos with free electrons. The emergence of neutrino-electron pairs should be accompanied by radio emission. Electrides can be transparent to radio waves. By placing capsules with an electride in a shielded container with an exit in the form of a waveguide, we obtain a detector of neutrino-electron interaction. The range of radio emission will be from a few MHz to several GHz.

4) Development of an electronic gallium neutrino detector operating in real time. The sensitive element of the detector will be gallium nitride nanotubes grown on a microchip. Such a detector will have increased sensitivity along the nanotubes and should outperform the radiochemical detectors Gallex, GNO, and SAGE.

5) Solar neutrinos and beta decay. If we assume that the solar core has a periodicity of several minutes, then the study of the influence of solar neutrinos on beta decay should be aimed at searching for periodicity in this time interval.

6) Analysis of the background of LIGO and Virgo interferometers in the frequency range 2.9-4.5 mHz and search for a gravitational signal with a period of 4.7 minutes. If we assume that the change in the solar neutrino flux between minimum and maximum is 20%, then the fluctuation in the mass of the sun will be 1 million tons, or 5×10^{-22} of the mass of the sun. The intensity of the gravitational signal corresponding to this oscillation is 5 orders of magnitude higher than that of the event GW170817. A constant signal of such power cannot be overlooked.

7) Fixation and analysis of the decay rate of the strontium aluminate afterglow to identify possible fluctuations. It is assumed that solar neutrinos can trigger phosphorescence.

8) Study of the glow pulsations of tropical fireflies. If solar neutrinos affect bioluminescence, and if there is an oscillation of their flux, then the pulsations of the glow of distant groups of fireflies should be synchronous.

9) Thorough study of solar radiation in the energy range 1-5 keV.

10) Study of the polarization of photons with an energy of 3.5 keV from the nearest galaxy clusters. In the spectra of galaxies, photons with a given energy can have polarization different from the rest of the spectrum. Mostly circular polarization (left or right) should correlate with the predominance of LM or anti-LM.

11) Collisions of accelerated protons with LM in the collider. It is assumed that on the LM side, Tt and Hx are mainly involved. Upon reaching a certain kinetic energy, the following reactions are possible:

$$p + Hx \rightarrow n + 2Du + \mu^{+} + \nu + something\ , \tag{14}$$

$$p + Tt \rightarrow n + Du + \mu^{+} + \nu + something\ , \tag{15}$$

$$p + Hx \rightarrow p + Du + \pi^{0} + \nu + \bar{\nu} + something\ , \tag{16}$$

$$p + Tt \rightarrow p + \pi^{0} + \nu + \bar{\nu} + something\ , \tag{17}$$

It is assumed that at the entrance to the process from the side of the LM nuclei, the mass of only one subunit of the nucleus (i.e., ~0.7 MeV) participates in the reaction with transformation. The calculated proton energy thresholds will be 151 and 195 GeV for the production of muon and pion, respectively. The actual threshold will be somewhat lower due to the symmetry of the LM nuclei. In reactions with muon production, only one neutrino of the LM nucleus undergoes transformation, and the rest of the neutrinos reduce the proton energy threshold by 5% of each neutrino. In reactions with pion production, two neutrinos undergo transformation simultaneously, and the rest of the neutrinos reduce the proton energy threshold together by 10%. At the exit, up to 43% of all energy is carried away by neutrinos, Du, and other particles. Table 4 shows the reaction energy parameters, and a comparison with the generally accepted interpretation of the observed events.

Table 4: Energy parameters in proton-LM collision reactions

Neutrinium element	Particle born	Actual threshold energy of protons	Standard interpretation of events
Hx	muon	~113 GeV	80.4 GeV, W boson
Tt	muon	~128 GeV	91.2 GeV, Z boson
Hx, Tt	pion	~176 GeV	125.2 GeV, Higgs boson

To confirm the reality of such collisions, it is necessary to launch the accelerator in the mode without collision of counter proton beams.

12) Study of the interaction of reactor antineutrinos near a pair of closely spaced reactors. Here it is necessary to determine whether the fusion of neutrino pairs is accompanied by radiation, and to select the spectral lines corresponding to the secondary synthesis of Tt, Hx. And also to establish to what extent antineutrinos of the earth's crust are involved in this interaction.

13) Deviation of solar neutrinos by an electron beam and detection of subsequent synthesis of LM. This requires a high current density electron gun and a soft X-ray receiver. Neutrinos will deflect upon interaction with the electron flux and form pairs. Part of the pairs will merge into Du.

14) Scanning the Earth with a Du flux created from solar neutrinos. The scanning Du flux is made as powerful as possible. In other places, the soft X-ray background is monitored to identify and measure the contribution of reflected Du to the synthesis of Tt, Hx.

15) Detection of LM annihilation in a strong magnetic field. A sealed transparent sphere with a vacuum inside is placed above the north or south pole of a neodymium magnet. On the opposite side, a winding is applied to the sphere, to which an alternating current is supplied with a frequency of tens of kHz (to enhance annihilation). At some distance optical, UV, X-ray and gamma detectors are located.

16) LM capture by Bose-Einstein condensate. The efficiency of trapping the LM nuclei is estimated by the change in the interference pattern.

17) Creation of thin-film structures based on Mott insulators, capable of trapping LM nuclei with nonzero spin, and verification of possible LM annihilation.

18) Making an aerogel from C12A7:e^- electride and testing its ability to capture LM.

19) LM flow management. Cooper electron pairs of the superconducting current may have the effect of LM drift. Superconductor–insulator–superconductor tunnel junctions (SIS) are used as control elements. Passing through SIS packets, LM nuclei flux can change the direction of motion in a given way.

20) Creation of an autonomous engine for interplanetary spacecraft operating on the LM annihilation. Accumulation of LM and anti-LM occurs in traps made from

aerogel. The same aerogel traps gases (hydrogen). Annihilation of LM is initiated by the induction of a magnetic field. The captured gases, receiving energy from the LM annihilation, evaporate in a given direction, imparting an impulse to the spacecraft.

9. Extragalactic Background Light

The extragalactic background light (EBL) is the second most powerful source of diffuse background radiation of the universe after cosmic microwave background radiation (CMBR). There is a hypothesis that the EBL appeared as a result of dispersion of gamma radiation of quasars in an interstellar medium. However, in our model it is assumed that the source of EBL was the synthesis of LM in the era of recombination, at z≈1089. According to observations, the spectral maximum of the EBL is at a wavelength of about 1200-1250 nm. Respectively, the photon energy at the time of emission was approximately 1.1 keV. This is the energy of synthesis of Tt, Hx from slow Du, Tt at a temperature of about 2970 K.

10. Conclusion

By telling ourselves that the hidden sector is difficult to access, we still believe that these difficulties can be overcome. To do this, we need to properly model the properties of the hidden sector. And if we have no idea what exactly these properties should be, then we need to consider as many different options as possible. This is exactly what has not yet happened with DM. Among the candidates considered to be the most promising, there are still not found: a) WIMPs with a mass of 10-1000 GeV, b) axions with a mass from 1 μeV to 1 eV, c) sterile neutrinos with a mass >1 eV. The gap is filled by the LM model with the mass of particles (or rather nuclei) commensurate with the rest mass of an electron. But does it not seem to us that this model is just one of the guesses of subjective opinion? Or, shall we say, is LM capable of claiming to be a conceptual scheme? We do not yet have an answer to this question, but we are trying to find an explanation for the known phenomena where LM could manifest itself. A simulation of scientific search arises, and we have new hypotheses, predictions and proposals for new experiments. Some of these experiments can be carried out today. Others require effort, but these efforts can be worthwhile.

Bibliography

[1] E. Bulbul, M. Markevitch, A. Foster, R. K. Smith, M. Loewenstein, S. W. Randall, Detection of An Unidentified Emission Line in the Stacked X-ray spectrum of Galaxy Clusters. ApJ 789, 13, arXiv:1402.2301, (2014)
[2] A. Boyarsky, O. Ruchayskiy, D. Iakubovskyi, J. Franse, An unidentified line in X-ray spectra of the Andromeda galaxy and Perseus galaxy cluster. Phys. Rev. Lett. 113, 25, arXiv:1402.4119, (2014)
[3] K. J. H. Phillips, B. Sylwester, J. Sylwester, The X-Ray Line Feature At 3.5 Kev In Galaxy Cluster Spectra. ApJ 809, 50, arXiv:1507.04619, (2015)
[4] J. P. Conlon, F. Day, N. Jennings, S. Krippendorf, M. Rummel, Consistency of Hitomi, XMM-Newton, and Chandra 3.5 keV data from Perseus. Phys. Rev. D 96, 123009, (2017), arXiv:1608.01684, (2016)
[5] D. Skripachov, A New Model of Gravitation. viXra:1404.0463, (2014)
[6] D. Skripachov, Virtual Crossword of Grand Unification. viXra:1405.0305, (2014)
[7] D. Skripachov, Two-Level Mass Model of the Milky Way. viXra:1408.0106, (2014)
[8] A. G. Cohen, A. De Rújula, and S. L. Glashow, A Matter-Antimatter Universe? ApJ 495 539, (1998),

arXiv:astro-ph/9707087, (1997)
[9] R. Jr. Davis, D. S. Harmer, Solar Neutrinos. Brookhaven National Laboratory, Upton, New York, (1965)
[10] J. N. Bahcall, M. H. Pinsonneault, S. Basu, Solar Models: current epoch and time dependences, neutrinos, and helioseismological properties. ApJ 555, 990, (2001), arXiv:astro-ph/0010346, (2001)
[11] J. N. Abdurashitov, et al., (SAGE Collaboration), Measurement of the solar neutrino capture rate with gallium metal. III: Results for the 2002--2007 data-taking period. Phys. Rev. C 80, 015807, arXiv:0901.2200, (2009)
[12] V. Antonelli, L. Miramontia, C. Peña-Garay, and A. Serenelli, Solar Neutrinos. Advances in High Energy Physics, vol. 2013, (2013), arXiv:1208.1356, (2012)
[13] E. Tandberg-Hanssen, A. G. Emslie, The physics of solar flares. Cambridge University Press, Cambridge, (1988)
[14] Zhu L., R.W. Schunk, and J.J. Sojka, Polar cap arcs: A review, Journal of Atmospheric and Terrestrial Physics 59, 1087, (1997)
[15] R. A. Howard, A Historical Perspective on Coronal Mass Ejections. Geophysical Monograph Series 165, 7, (2006)
[16] Iain G. Hannah, G. J Hurford, H. S. Hudson, R. P. Lin, K. van Bibber, First limits on the 3-200 keV X-ray spectrum of the quiet Sun using RHESSI. ApJ Letters 655, arXiv:astro-ph/0702726, (2007)
[17] L. Wolfenstein, Neutrino oscillations in matter. Phys. Rev. D 17, 2369, (1978)
[18] A. Yu. Smirnov, The MSW effect and Solar Neutrinos, 10th workshop on Neutrino Telescopes, Venice, arXiv:hep-ph/0305106, (2003)
[19] M. Deen, E. Wielandt, E. Stutzmann, W. Crawford, G. Barruol, K. Sigloch, First observation of the Earth's permanent free oscillations on ocean bottom seismometers. Geophysical Research Letters 44, (2017)
[20] T. V. Zaqarashvili, K. Murawski, M. L. Khodachenko, D. Lee, The excitation of 5-min oscillations in the solar corona. A&A 529, A85 (2011)
[21] C. P. Barrington-Leigh, U. S. Inan, M. Stanley, Identification of sprites and elves with intensified video and broadband array photometry. J. Geophys. Res. Space Physics, 106, 1741, (2001)
[22] T. Gjesteland, N. Østgaard, P. Bitzer, H. J. Christian, On the timing between terrestrial gamma ray flashes, radio atmospherics, and optical lightning emission. J. Geophys. Res. Space Physics, 122, 7734, (2017)
[23] J. Hanasz, H. de Feraudy, R. Schreiber, and M. Panchenko, Pulsations of the auroral kilometric radiation. Journal of Geophysical Research: Space Physics 111, A3, (2006)
[24] A. Bhardwaj, X-Ray Emission from Jupiter, Saturn, and Earth: A Short Review. Advances in Geosciences 3, 215, arXiv:astro-ph/0605282, (2006)
[25] W. R. Dunn, et al., The impact of an ICME on the Jovian X-ray aurora. J. Geophys. Res. Space Physics, 121, 2274, (2016)
[26] A. A. Deshpande, J. M. Rankin, Pulsar Magnetospheric Emission Mapping: Images and Implications of Polar-Cap Weather. ApJ 524, 1008, arXiv:astro-ph/9909398, (1999)
[27] O. Maron, J. Kijak, M. Kramer, R. Wielebinski, Pulsar spectra of radio emission. A&A Suppl. Ser. 147, 195-203, arXiv:astro-ph/0010233, (2000)
[28] T. J.-L. Courvoisier, The Bright Quasar 3C 273. A&A Rev. 9, 1-32, arXiv:astro-ph/9808147, (1998)
[29] Y. Shen , M. A. Strauss, N. P. Ross, et al., Quasar Clustering from SDSS DR5: Dependences on Physical Properties. ApJ 697, 1656, (2009), arXiv:0810.4144, (2008)
[30] M. Haverkorn, V. Heesen, Magnetic fields in galactic haloes. Space Science Reviews 166, 133, (2012), arXiv:1102.3701, (2011)
[31] R. Beck, R. Wielebinski, Magnetic fields in galaxies. Planets, Stars and Stellar Systems 5 641, arXiv:1302.5663, (2013)
[32] Z. Berezhiani, A. D. Dolgov, I. I. Tkachev, Dark matter and generation of galactic magnetic fields. EPJC 73, 2620, arXiv:1307.6953, (2013)
[33] D. L. Meier, The Theory and simulation of relativistic jet formation: Towards a unified model for micro- and macroquasars. New Astron.Rev. 47, arXiv:astro-ph/0312048, (2003)
[34] Space environment (natural and artificial) -- Earth upper atmosphere. ISO/FDIS 14222, www.iso.org, (retrieved in 2013)
[35] S Pommé, The uncertainty of the half-life. Metrologia 52, S51, (2015)
[36] E. Bellotti, C. Broggini, G. Di Carlo, M. Laubenstein, R. Menegazzo b, Search for time modulations in the decay constant of 40 K and 226 Ra at the underground Gran Sasso Laboratory. Physics Letters B 780, 61-65, arXiv:1802.09373, (2018)
[37] K. Eguchi, et al., (KamLAND Collaboration), First Results from KamLAND: Evidence for Reactor Anti-Neutrino Disappearance. Phys. Rev. Lett. 90, 021802, (2003), arXiv:hep-ex/0212021, (2002)
[38] M. M. Nieto, A. C. Hayes, C. M. Teeter, W. B. Wilson, W. D. Stanbro, Detection of Antineutrinos for Non-Proliferation. Nucl. Sci. Engin. 149, 270, (2005), arXiv:nucl-th/0309018, (2004)
[39] F. P. An, et al., (Daya Bay Collaboration), Improved Measurement of Electron Antineutrino Disappearance at Daya Bay. Chinese Phys. C 37, 011001, (2013), arXiv:1210.6327, (2012)

[40] P. D. Ewing, S. W. Kercel, K. Korsah, R. T. Wood, Electromagnetic Compatibility in Nuclear Power Plants. Global '99: International Conference on Future Nuclear Systems, Jackson Hole, WY, (1999)
[41] M. Tanabashi et al. (Particle Data Group), Review of Particle Physics. Phys. Rev. D 98, 030001, (2018)
[42] L. W. Clark, A. Gaj, L. Feng, C. Chin, Collective emission of matter-wave jets from driven Bose-Einstein condensates. Nature 551, 356, arXiv:1706.05560, (2017)
[43] E. Y. Cho, H. Li, S. A. Cybart, Direct-Write Ion Beam Irradiated Josephson Junctions. arXiv:1906.10328, (2019)
[44] B. P. Abbott, et al., (LIGO Scientific Collaboration and Virgo Collaboration, Fermi Gamma-ray Burst Monitor, and INTEGRAL), Gravitational Waves and Gamma-Rays from a Binary Neutron Star Merger: GW170817 and GRB 170817A. ApJL 848 L13, (2017)
[45] R. G. Leigh, Ph. Phillips, T.-P. Choy, Hidden Charge 2e Boson in Doped Mott Insulators: Field Theory of Mottness. Phys. Rev. Lett. 99, 046404, (2007), arXiv:cond-mat/0612130, (2007)
[46] M. Sasao, at al., Negative-hydrogen-ion production from a nanoporous 12CaO·7Al2O3 (C12A7) electride surface. Appl. Phys. Express 11, 066201, (2018), arXiv:1911.11007, (2018)
[47] R. H. Frisbee, How to Build an Antimatter Rocket for Interstellar Missions: Systems level Considerations in Designing Advanced Propulsion Technology Vehicles. AIAA Paper 2003-4696, (2003)
[48] M. G. Hauser, The Far Infrared and Submillimeter Diffuse Extragalactic Background. ASP Conf. Ser. 204, 101, arXiv:astro-ph/0105550, (2001)
[49] K. Mattila, K. Lehtinen, P. Vaisanen, G. von Appen-Schnur, C. Leinert, Spectrophotometric measurement of the Extragalacic Background Light . IAU Symposium 284, arXiv:1111.6747, (2001)
[50] H. Abdalla, et al., (H.E.S.S. Collaboration), Measurement of the EBL spectral energy distribution using theVHE γ-ray spectra of H.E.S.S. blazars. A&A 606, A59, arXiv:1707.06090, (2017)
[51] V. A. Acciari, at al., (MAGIC Collaboration), Measurement of the Extragalactic Background Light using MAGIC and Fermi-LAT gamma-ray observations of blazars up to z = 1. arXiv:1904.00134v1, (2019)
[52] D. Davidson, On the Very Idea of a Conceptual Scheme. Proceedings and Addresses of the American Philosophical Association, 47, (1973)